frontiers | Frontiers in Materials

ORIGINAL RESEARCH
published: 05 May 2022
doi: 10.3389/fmats.2022.894061

Carbon Aerogels From Softwood Kraft Lignin for High Performance Supercapacitor Electrodes

Muzaffer A. Karaaslan[1], Li-Ting Lin[2], Frank Ko[2] and Scott Renneckar[1]*

[1]*Advanced Renewable Materials Laboratory, Department of Wood Science, The University of British Columbia, Vancouver, BC, Canada,* [2]*Department of Materials Engineering, The University of British Columbia, Vancouver, BC, Canada*

Porous carbon materials derived from plant biomass offer great promise towards developing sustainable and advanced renewable materials for energy applications. Lignin is as an abundant and renewable aromatic biopolymer with high carbon content and chemical functionality for crosslinking, which make lignin a promising alternative for environmentally-friendly carbon aerogel production. In this study, carbon aerogels were produced using an industrial softwood kraft lignin isolated from renewable forest resources. Crosslinked lignin gels were synthesized using an epoxy compound and converted into carbon aerogels with subsequent sol-gel processing, supercritical drying and pyrolysis steps. The effect of lignin-to-crosslinker ratio on the chemical, physical and structural properties of resulting carbon aerogels were investigated. The bulk density of carbon aerogels increased as the lignin content increased from 56 wt% to 87 wt% and ranged from 0.45 to 0.83 g/cm^3, respectively. FTIR results showed that crosslinked network structure was promoted when the lignin-to-crosslinker ratio was higher, which impacted the porous texture of resulting carbon aerogels as evidenced by SEM analysis. XRD analysis was used to correlate degree of graphitization and lignin content, which impacted the electrical conductivity and ion-charge transfer in carbon electrodes. To evaluate the hierarchical porous structure and determine the BET surface area and pore volume, N_2 and CO_2 gas adsorption experiments were conducted. Carbon aerogels with 81 wt% and 87 wt% lignin had superior structural characteristics, which further improved with surface activation with KOH resulting in 1,609 m^2/g for BET surface area, 0.98 cm^3/g for total pore volume and 0.68 cm^3/g for micropore volume. The electrochemical tests of electrodes assembled from 87 wt% lignin carbonized sample with a specific capacitance of 122 F/g at 1A/g had better performance compared to a commercial activated carbon (74 F/g with 845 m^2/g BET) and resorcinol-formaldehyde based carbon aerogel (61 F/g with 1,071 m^2/g BET area), while maintaining ~90% of its capacitance after 5,000 charge-discharge cycles. Surface activation of lignin carbon aerogels further boosted the capacitance properties, an outstanding energy density of 3.2 Wh/kg at 209.1 W/kg power density were obtained for the supercapacitor electrodes built from the A-CA-L87 activated carbon aerogel.

Keywords: lignin, biomass, carbon aerogel, activation, crosslinking, epoxy, supercapacitor, electrode

OPEN ACCESS

Edited by:
Erlantz Lizundia, University of the Basque Country, Spain

Reviewed by:
Maurice Collins, University of Limerick, Ireland
Noriko Yoshizawa, National Institute of Advanced Industrial Science and Technology (AIST), Japan

****Correspondence:***
Muzaffer A. Karaaslan
muzaffer.karaaslan@ubc.ca

Specialty section:
This article was submitted to Energy Materials, a section of the journal Frontiers in Materials

Received: *11 March 2022*
Accepted: *20 April 2022*
Published: *05 May 2022*

Citation:
Karaaslan MA, Lin L-T, Ko F and Renneckar S (2022) Carbon Aerogels From Softwood Kraft Lignin for High Performance Supercapacitor Electrodes. Front. Mater. 9:894061. doi: 10.3389/fmats.2022.894061

INTRODUCTION

In recent decades, the need for reliable energy storage systems has increased with the progress of sustainable and renewable energy technologies and the increasing demand for consumer electronics and electric vehicles. Energy storage systems that allow more efficient use of energy and power are crucial for stable and continuous energy supply. Supercapacitors (SCs) or electrochemical double layer capacitors (EDLCs) are one major class of electrical energy storage devices that offer a great promise because of their high-power capabilities, fast charge-discharge capacity, long cycle-life and safety (Jin et al., 2018; Ma et al., 2021). Compared to rechargeable batteries relying on chemical reactions, SCs store energy electrostatically and can be charged and discharged at faster rates (specific power up to 10^4 W/kg in less than 1 min) for up to ~10^6 cycles (Raza et al., 2018). On the other hand, SCs can provide a limited specific energy of 1–10 Wh/kg which is several orders of magnitude lower than Li-ion batteries (10–100 Wh/kg) (González et al., 2016). As a result, SCs are suitable for applications where improved power efficiency is needed such as for industrial power and energy management, back-up power systems, regenerative brake systems in hybrid electric vehicles, portable electronic devices (Deka et al., 2017; Palchoudhury et al., 2019). Typically, a SC cell is composed of two carbon electrodes soaked in electrolyte and a polymer membrane separator in between them. Carbon materials such as activated carbons, carbon fibers, carbon aerogels, carbon nanotubes, graphene are widely used as the active component in SC electrodes due to their high surface area, porosity, electrical conductivity, and chemical stability (Tao et al., 2013; Wang Q. et al., 2016; Chen et al., 2017; Ma et al., 2021). Among them, carbon aerogels have been extensively studied as SC electrodes thanks to their tunable three-dimensional interconnected porous structure, hierarchical porosity, high specific surface area and electrical conductivity (Biener et al., 2011; Antonietti et al., 2014; Li F. et al., 2019). To construct the unique porous structure of carbon aerogels, highly reactive phenolic precursors such as resorcinol, phenol and melamine are commonly used and reacted with crosslinkers such as formaldehyde in a controlled manner, followed by subsequent sol-gel processing, supercritical drying and carbonization stages (Tamborini et al., 2017; Li F. et al., 2019). However, these precursors are toxic, expensive, and derived from petroleum-based non-renewable resources. There have been great efforts in literature for finding renewable alternatives and replacing these precursors with readily available environmentally friendly raw materials from biomass sources (Gao et al., 2017; Jin et al., 2018; Castro-Gutiérrez et al., 2020; Sam et al., 2020).

Lignin, as the second most abundant biopolymer after cellulose, is one of the three main components of all plant biomass and industrially available in potentially large quantities as a by-product of pulping mills and bio-refineries. As a bio-based feedstock, lignin has a great potential and various lignin valorization pathways have been proposed (Ragauskas et al., 2014; Collins et al., 2019). Owing to its aromatic nature, chemical functionality, thermal stability, high carbon content and low cost, lignin is a promising resource for producing carbon aerogels as well as for other carbon-based materials such as carbon fibers and activated carbon for energy applications (Baker and Rials, 2013; Xu et al., 2018; Geng et al., 2020; Zhu et al., 2020; Culebras et al., 2022). Recent studies on lignin-based carbon aerogels focused on partial or full replacement of resorcinol or phenol with lignin and using formaldehyde for crosslinking and polycondensation reactions due to its low cost and high reactivity (Grishechko et al., 2013b; Xu et al., 2015, 2018; Yang et al., 2017). To form a crosslinked gel network, formaldehyde both reacts with resorcinol and lignin forming methylene and methylene ether linkages, however, in the absence of resorcinol, the reaction takes place very slowly (3–5 days) due to steric hindrance from the highly substituted aromatic rings of lignin (Chen et al., 2011; Grishechko et al., 2013b). Moreover, formaldehyde is a toxic and carcinogenic substance and recent toxicology regulations in North America and Europe suggest to limit the use of formaldehyde or its total replacement with alternative chemicals, especially from phenolic-based resins and adhesives (Rovira et al., 2016; Mundt et al., 2018).

In this work, we study the preparation of lignin-based carbon aerogels by an alternative crosslinking strategy without using formaldehyde, resorcinol, and phenol. Using an industrial softwood kraft lignin and an epoxy compound, we fabricated low-cost carbon aerogels from forest-biomass suitable for energy storage applications, specifically as carbon electrodes for supercapacitors. We studied the effect of lignin-to-crosslinker ratio on the chemical, physical, and structural properties and compared the SC performance of lignin carbon aerogels with a commercial resorcinol-formaldehyde (RF)-based carbon aerogel and an activated carbon. In addition, we evaluated the impact of chemical surface activation of carbon aerogels with an alkaline activator (KOH) on the structural properties and SC performance.

MATERIALS AND METHODS

Materials

Softwood kraft lignin produced from southern pine (BioChoice™) was provided by Domtar Inc. All other reagents were ACS grade and used as is. Total hydroxyl group content of lignin was ~5 mmol/gr as determined by ^{31}P NMR (Liu et al., 2020).

Preparation of Lignin Carbon Aerogels

Lignin was dissolved at a 30 wt% concentration in 1 M sodium hydroxide (NaOH) and stirred overnight at room temperature for complete dissolution. Epichlorohydrin at different molar ratios (epichlorohydrin: lignin: 0.6:1, 1:1, 1:2, 1:3, corresponding to 44: 56, 32:68, 19:81, 13:87 w/w %/% ratio) was added into lignin solution and stirred for 15 min. The mixtures were transferred into glass vials, sealed, and placed in an oven preheated at 75°C for 24 h. After the crosslinking reaction and gel formation, lignin gels were carefully removed from glass vials, rinsed, and solvent-exchanged by keeping the gels in distilled water and absolute ethanol sequentially for 3 days each, by exchanging with fresh solvent two times a day. Lignin gels in ethanol (alcogels) were

supercritical-dried with liquid carbon dioxide using Tousimis Autosamdri 815B Critical Point Dryer. To produce carbon aerogels (CA), lignin aerogels were heat-treated in a tube furnace from room temperature to 900°C with a heating rate of 5°C/min and at 900°C for 1 h under nitrogen gas flow. For production of activated carbon aerogels (A-CA), CA samples were immersed into 6 M potassium hydroxide solution (3:1 KOH: lignin w/w), dried in oven at 105°C, and heated in a tube furnace at 800°C for 1 h under a nitrogen gas flow. After heat processing, A-CA samples were neutralized with 0.1 N hydrochloric acid (HCl), thoroughly washed with distilled water to remove residual impurities, and dried in oven at 105°C.

Characterizations

The morphology of lignin-based carbon aerogels was analyzed by field emission scanning electron microscopy (FE-SEM, Hitachi 4,700) at accelerating voltage of 5 kV. The samples were mounted onto metal holders with carbon tape, and sputter-coated with gold. To evaluate the crystal structure of carbon aerogels, X-ray diffraction patterns were collected in the range of from $2\theta = 5^{\circ}$ to $2\theta = 60^{\circ}$ at a CuKα radiation wavelength of $\lambda = 1.5406^{\circ}$ from a generator operating at 40 kV and 40 mA. The pore volume, surface area and pore size distributions of lignin-based carbon aerogels were determined from nitrogen (N_2, 77 K) adsorption-desorption and carbon dioxide (CO_2, 273 K) adsorption isotherms using Micromeritics 3Flex physisorption analyzer. Samples were degassed under vacuum at 350°C for 6 h prior to gas sorption experiments. The total pore volume (V_t) was obtained from the nitrogen adsorption isotherm at p/p_0 ~0.99 and the specific surface area (S_{BET}) was determined using the Brunauer-Emmett-Teller (BET) method. The micropore volume (V_{micro}) was calculated using t-plot analysis. The pore size distributions and average pore diameter is determined from the N_2 desorption branch using Barrett, Joyner, and Halenda (BJH) method. In addition, micropore volume and pore size distributions of ultramicropores (pore size < 1 nm) were analyzed from the CO_2 adsorption isotherm ($V_{micro\text{-}CO2}$) using Dubinin-Radushkevich equation and DFT models. The bulk density (ρ, g/cm^3) was calculated by dividing the mass of the sample to its volume for all aerogels after supercritical drying and carbonization. Fourier transform infrared (FTIR) spectra of lignin aerogels and carbon aerogels were recorded from 600 to 4,000 cm^{-1} at a resolution of 4 cm^{-1} using a Bruker Invenio spectrometer.

The electrochemical experiments were conducted in a two-electrode configuration with stainless steel current collectors, a polyvinylidene fluoride (PVDF) filter paper as the separator, and 1.0 M H_2SO_4 as the aqueous electrolyte at room temperature. Carbon electrodes were prepared from a slurry of finely ground lignin carbon aerogel, carbon black, and the PVDF binder with the mass ratio of 8:1:1 dispersed in N-methyl pyrrolidone (NMP) solution. An equal amount of slurry was coated on metal collectors (area:1 cm^2), dried in an oven at 105°C for at least 24 h, and immersed in electrolyte prior to the electrode assembly. Electrochemical tests including cyclic voltammetry (CV), galvanostatic charge-discharge (GCD), and electrochemical impedance (EIS) were carried out using the Gamry Interface 1010 E potentiostat workstation with the operation potential from 0–0.8 V. CV tests were conducted with different scan rate from 5 to 200 mV/s. The GCD tests were investigated at a current density of 0.1, 0.5, and 1 A/g, respectively. EIS tests were conducted in the frequency range of 10^{-1}–10^6 Hz to understand the resistance of the electrode.

The specific capacitance (C_s) of the single electrode were calculated from the CV curve by **Eq. 1**.

$$C_S = \frac{2 \times \int IVdV}{m \times v \times \Delta V} \tag{1}$$

where I, V, m, v, and ΔV are the current, potential, electrode mass, scan rate, and operating voltage window, respectively.

The specific capacitance (C_s) for the single electrode was also calculated from the discharge curve by **Eq. 2**.

$$C_S = \frac{4 \times I \times \Delta t}{m \times \Delta V} \tag{2}$$

where I, Δt, m, ΔV are the discharge current, the discharge time, the total mass of the electrode materials in both working electrodes, and the operating voltage range, respectively.

The energy density (E; Wh/kg) and power density (P; W/kg) were calculated from **Eqs. 3**, **4**

$$E = \frac{C_S \times \Delta V^2}{8 \times 3.6} \tag{3}$$

$$P = \frac{3600 \times E}{\Delta t} \tag{4}$$

where C_S, ΔV, Δt is the specific capacitance from the GCD curve, the operating voltage range, and discharge time, respectively.

RESULTS AND DISCUSSION

Synthesis of Aerogels From Lignin

In this study, biomass-derived carbon aerogels were produced from a commercially available lignin isolated by the kraft pulp processing of softwood species. Kraft lignin has various functional groups such as aromatic/aliphatic hydroxyl, carboxylic acid and carbonyl groups that are reactive towards chemical derivatization and copolymerization (Glasser, 2019). By taking advantage of lignin's aromatic nature and chemical functionality, cross-linked network gels were synthesized and converted into aerogel materials by subsequent sol-gel processing, supercritical drying and pyrolysis stages (**Figure 1**). To synthesize lignin gels, lignin was first solubilized under aqueous alkaline conditions, which makes the aromatic hydroxyl groups charged (phenoxy ion) and active, and reacted with an industrially used epoxy compound, epichlorohydrin. The suggested reaction mechanism between lignin and epichlorohydrin (**Figure 1**) includes an ring-opening of oxirane ring followed by epoxidation of hydroxyl groups of lignin, and reaction of an epoxidized lignin with another lignin anion, resulting in the crosslinking of lignin macromolecules (Saidane et al., 2010; Nypelö et al., 2015). FT-IR spectra of lignin and aerogels with different lignin contents confirmed the structural changes of

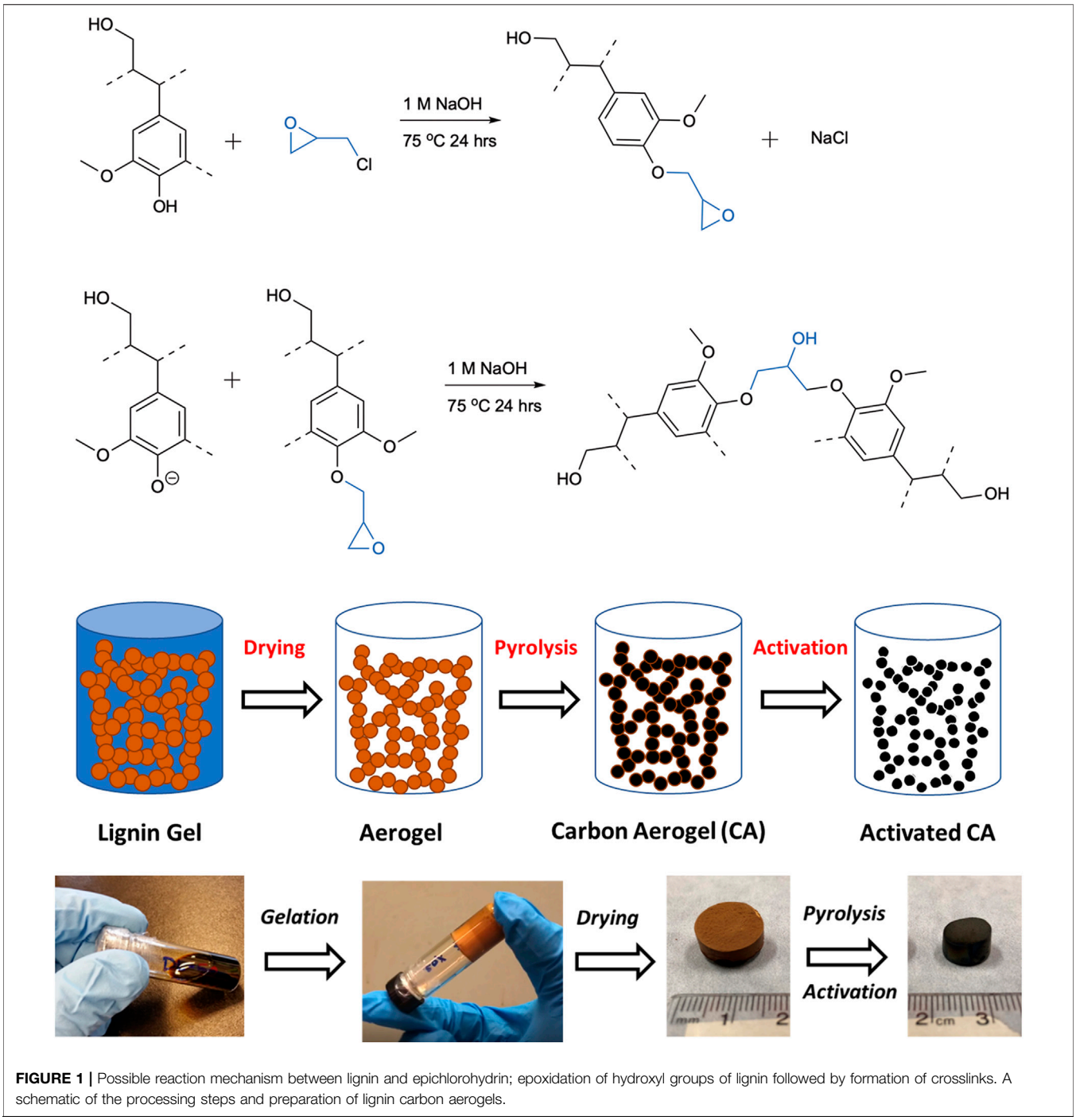

FIGURE 1 | Possible reaction mechanism between lignin and epichlorohydrin; epoxidation of hydroxyl groups of lignin followed by formation of crosslinks. A schematic of the processing steps and preparation of lignin carbon aerogels.

lignin after crosslinking reaction (**Figure 2**). The peaks characteristic to lignin's hydroxyl (O-H) stretching at 3,400 cm^{-1} and aromatic skeletal vibrations at 1,595 cm^{-1} and 1,510 cm^{-1} shifted in the spectra of all aerogels after the reaction. For the region corresponding to C-H stretching of methyl and methylene groups, the intensity of 2,935 cm^{-1} peak increased and a new peak appeared at 2,877 cm^{-1}. In addition, the peak at 1,365 cm^{-1} that belong to bending of phenolic hydroxyl groups of lignin disappeared and intensity of strong peaks at 1,125 cm^{-1} and 1,085 cm^{-1} increased, confirming the crosslinking reaction and formation of ether (C-O-C) linkages (Passauer et al., 2012; Nypelö et al., 2015). The peak belonging to carbonyl stretching of unconjugated groups of lignin shifted from ~1710 cm^{-1} to ~1730 cm^{-1} only for L-56 and L-68 aerogels, which also suggested epoxidation of carboxyl acid groups of lignin. For aerogels with higher crosslinker content (44 and 32%), the peak that belongs to the oxirane ring appeared at 750 cm^{-1} while it disappeared for the aerogels with reduced amount of

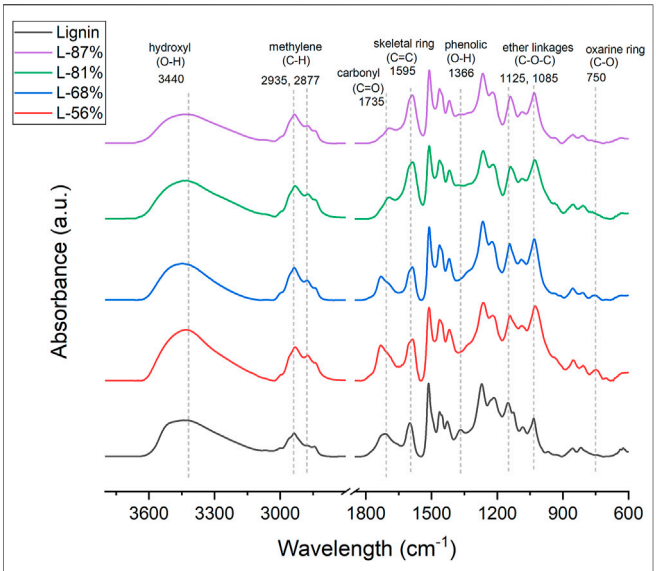

FIGURE 2 | FTIR spectra of lignin aerogels with different crosslinker-to-lignin ratios corresponding to 44, 68, 81, and 87 wt% of lignin (all spectra normalized with skeletal vibration band of lignin at 1,510 cm^{-1}).

crosslinker (19 and 13%). This observation is in agreement with previous studies that the higher crosslinker-to-lignin ratio favoured epoxidation of lignin over crosslinking while reducing the amount of crosslinker resulted in more crosslinked structure (Saidane et al., 2010; Nypelö et al., 2015).

After formation of the crosslinked network structure, lignin gels (hydrogels) were kept in water for several days to remove unreacted components and converted into "alcogels" in ethanol by repetitive solvent exchange steps. This step is critical as ethanol is miscible with liquid carbon dioxide, which reduces the surface tension and interfacial capillary forces within the pores, decreases the collapse of pore structure and excessive pore shrinkage upon removal of solvent during supercritical drying (Grishechko et al., 2013a; Baldino et al., 2020). The bulk density and porosity of aerogels and carbon aerogels prepared with different lignin-to-crosslinker ratios are shown in **Table1**. The porosity was calculated based on the ratio of bulk density of aerogels and skeletal density of lignin (1.4 g/cc) and amorphous carbon (2.0 g/cc) (Szczurek et al., 2011; Grishechko et al., 2013b). The bulk density of aerogels was in the range of 0.20 g/cm^3 to 0.74 g/cm^3, increased after carbonization, and ranged from 0.48 g/cm^3 to 0.83 g/cm^3 for carbon aerogels due to the combination of volumetric shrinkage and mass loss during pyrolysis. Increasing the amount of lignin relative to epichlorohydrin increased the bulk density of aerogels while reducing the porosity, which varied from 47% to 86%-- these data were similar to reported values for biobased aerogels prepared from lignin-phenol-formaldehyde and condensed tannin (Szczurek et al., 2011; Grishechko et al., 2013a, 2013b). These results suggested that the number of crosslinks reduced with the decreasing lignin-to-crosslinker ratio, resulting in weaker internal pore structure and higher shrinkage during drying process, therefore yielding higher bulk density. Note that porous carbon materials with higher bulk density enable higher packing density of active component in electrodes, which is desirable for high performance energy storage applications such as supercapacitors with outstanding volumetric capacitance (Tao et al., 2013; Wang Q. et al., 2016; Jin et al., 2018). In addition, due to high carbon content (60–65%) of lignin, the overall carbon yield of aerogels increased from 35 wt % to 47 wt% as the lignin content increased from 56 wt% to 87 wt %, which is an important criteria for the production of low-cost and high-yield electrodes from renewable carbon.

X-ray analysis of carbon aerogels showed that all samples had similar diffraction patterns characteristic to amorphous disordered carbon (**Figure 3**). The broad peaks at $2\theta = 23^{\circ}$ and $2\theta = 43^{\circ}$ corresponds to the d_{002} and d_{101} interlayer spacings of graphite, respectively (Xu et al., 2018). Also, the weak peak observed at about $2\theta = 12^{\circ}$ might be due to the presence of residual oxygenated groups (Li J. et al., 2019) due to partial graphitization of lignin at 900°C as revealed by elemental analysis and FTIR results (data not shown). However, it is likely that this weak peak might be related to the porous structure of carbon aerogels and the presence of nanopores which are less than 1 nm (Meynen et al., 2009; Zhang et al., 2017). The d_{002} interlayer spacing of carbon aerogels were slightly decreased from 4.01 Å to 3.88 Å with increasing lignin content, indicating that the CA-L87 carbon aerogel had higher degree of graphitization and improved stacking structure compared to the CA-L56 (Xu et al., 2018).

The surface morphology and porous structure of carbon aerogels prepared with different lignin-to-crosslinker ratios were examined by SEM (**Figure 4**). Depending on the composition of aerogels, the structure of pores and the

TABLE 1 | Bulk density and porosity of lignin-based aerogels and carbon aerogels prepared with different lignin-to-crosslinker ratios.

		Lignin-to-crosslinker ratio (w/w %)			
		0.6:1* (56:44)	**1:1* (68:32)**	**2:1* (81:19)**	**3:1* (87:13)**
Bulk density (g/cm^3)	Aerogel	0.20 ± 0.03	0.42 ± 0.05	0.45 ± 0.01	0.74 ± 0.01
	Carbon aerogel	0.48 ± 0.02	0.59 ± 0.06	0.74 ± 0.01	0.83 ± 0.03
Porosity (%)	Aerogel	86 ± 5	70 ± 4	68 ± 4	47 ± 3
	Carbon aerogel	76 ± 3	71 ± 3	63 ± 1	59 ± 2

**Molar ratio of lignin-to-epichlorohydrin based on total hydroxyl group of lignin (5 mmol/g).*

shape of carbon particles changed significantly. The samples with lower lignin-to-crosslinker ratios (CA-L87 and CA-L81) showed a three-dimensional porous network structure composed of interconnected particles (**Figures 4A–D**), which is typical for carbon aerogels with mesopores (2–50 nm) (Szczurek et al., 2011; Li F. et al., 2019). On the other hand, the samples CA-L68 and CA-L56 had no visible mesoporous network structure but composed of either spherical carbon particles with sizes ranging from 1–3 µm or micron-size pores (**Figures 4E–G**). Interestingly, higher magnification SEM images revealed that CA-L68 and CA-L56 samples had secondary carbon particles with less than 50 nm and additional surface features suggesting the presence of micropores (**Figures 4F–H**). This difference in the surface morphology might be explained by the changes in the chemical structure of lignin as revealed by FTIR analysis, which showed the presence of epoxidized lignin derivative in aerogels especially when the crosslinker ratio was higher. Prior to the formation of a fully crosslinked network, lignin's hydroxyl groups are first derivatized with epoxy functionality, which increases the free volume of lignin and therefore reduces its glass transition temperature and increasing its ability to flow at elevated temperatures. Thus, it is conjectured the formation of larger size primary carbon particles and the absence of observable mesoporous network in CA-L68 and CA-L56 samples might be due to the thermal flow and fusion of epoxidized lignin particles during carbonization process. These results suggested that a thermal-stabilization step of aerogels prior to carbonization, especially for the aerogels with higher content of epoxidized lignin derivatives, would prevent thermal fusion of particles and therefore maintain the mesoporous structure (Nypelö et al., 2015).

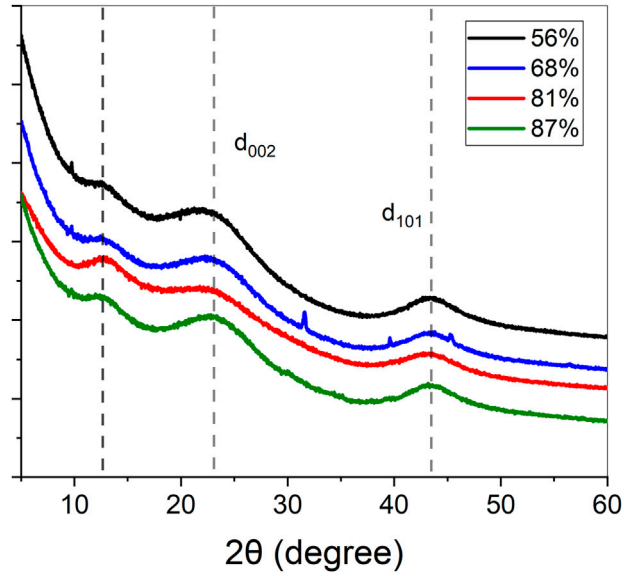

FIGURE 3 | X-ray diffraction patterns of lignin carbon aerogels with different crosslinker-to-lignin ratios corresponding to 44, 68, 81, and 87 wt% of lignin.

To better understand the porous structure of lignin carbon aerogels, nitrogen (N_2) adsorption-desorption isotherms were collected and the BET surface area, pore volume, average pore diameter and pore size distributions of all samples were calculated (**Figures 5A,C**; **Table2**). CA-L87 and CA-L81 samples had significantly higher BET surface areas (154 and 397 m^2/g) and total pore volumes (0.26 and 0.21 g/cm^3) compared to those of CA-L68 and CA-L56 samples, which is in accordance with the SEM observations. In addition, the hysteresis loop between adsorption and desorption branches and the pore size distribution curves obtained by the BJH method confirmed the presence of mesopores (2–50 nm), especially with the CA-L87 sample (**Figure 5C**). Interestingly, CA-L81 samples showed significantly higher micropore volume and surface area, as calculated by t-plot method, whereas CA-L87 had higher external surface area for meso- and macropores. On the contrary of the SEM images at higher magnifications, suggesting microporosity, N_2 adsorption results showed insignificant amount of micropores especially for of CA-L68 and CA-L56 samples. N_2 adsorption is the most used technique for the characterization of porous carbon materials, however, it has drawbacks for characterization of smaller micropores (<1 nm) due to limited diffusion rate of nitrogen at cryogenic temperatures (77K) (Thommes and Cychosz, 2014; Ambroz et al., 2018). Alternatively, CO_2 adsorption at 273K has become a common practice to characterize microporous carbons because of its of higher saturation pressure and ease of access to smaller micropores with sizes down to 0.35 nm (Thommes and Cychosz, 2014; Ko et al., 2021). The micropore volumes were calculated using the Dubinin-Radushkevich equation and the distribution of pores for the ultra-micropore region was obtained by the DFT models (**Figure 5E**; **Table2**). The results revealed that all samples had significant amount of pore volume in the range of 0.27–0.29 g/cm^3 for the pore sizes of about 0.5 and 0.8 nm.

To further improve the pore volume and surface area of carbon aerogels, KOH chemical activation process was used, which is a frequently used method for porous carbon materials in energy applications (Romanos et al., 2011; Wang and Kaskel, 2012). KOH reacts with carbon through redox reactions at elevated temperatures above 400°C, resulting in etching of carbon framework and development of porosity through formation of H_2O and CO_2. In addition, metallic potassium compounds formed during activation expands the carbon lattices, creating higher microporosity and surface area upon removal of metallic K by washing after activation process (Romanos et al., 2011; Wang and Kaskel, 2012). N_2 adsorption isotherms and pore size distribution of activated samples are shown in **Figure 5B** and **Figure 5D** and the structural properties of activated samples (A-CA) calculated from the N_2 and CO_2 adsorption isotherms were summarized in **Table2**. After surface activation, the BET surface area, total pore volume, and micropore volumes of all carbon aerogel samples improved considerably with values reaching up to 1,609 m^2/g and 0.98 cm^3/g with 0.68 cm^3/g, respectively. All samples showed substantial amount of

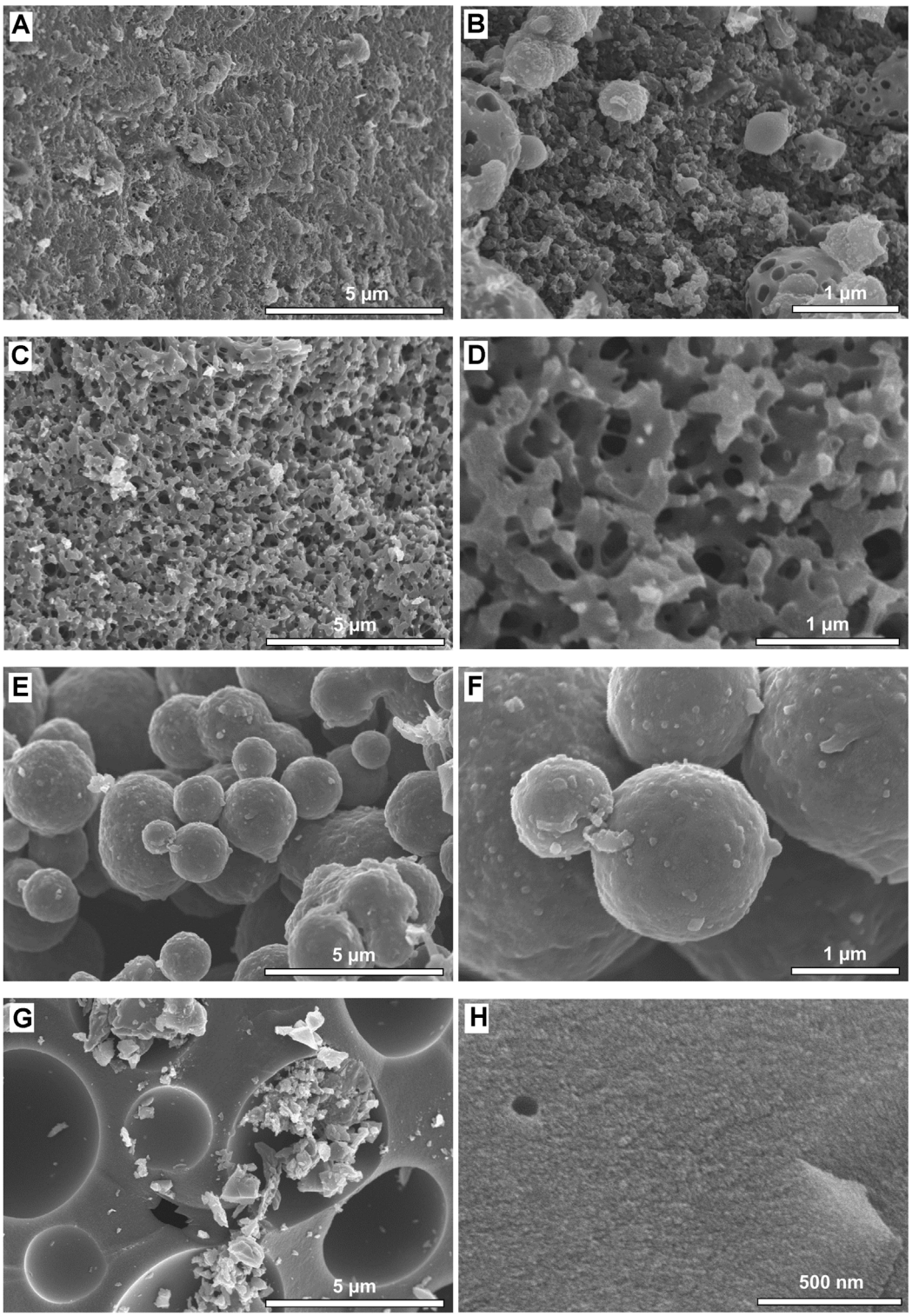

FIGURE 4 | SEM images of lignin carbon aerogels; **(A,B)** CA-L87, **(C,D)** CA-L81, **(E,F)** CA-L68, and **(G,H)** CA-L56, showing the effect of lignin content on surface morphology microstructure and porosity.

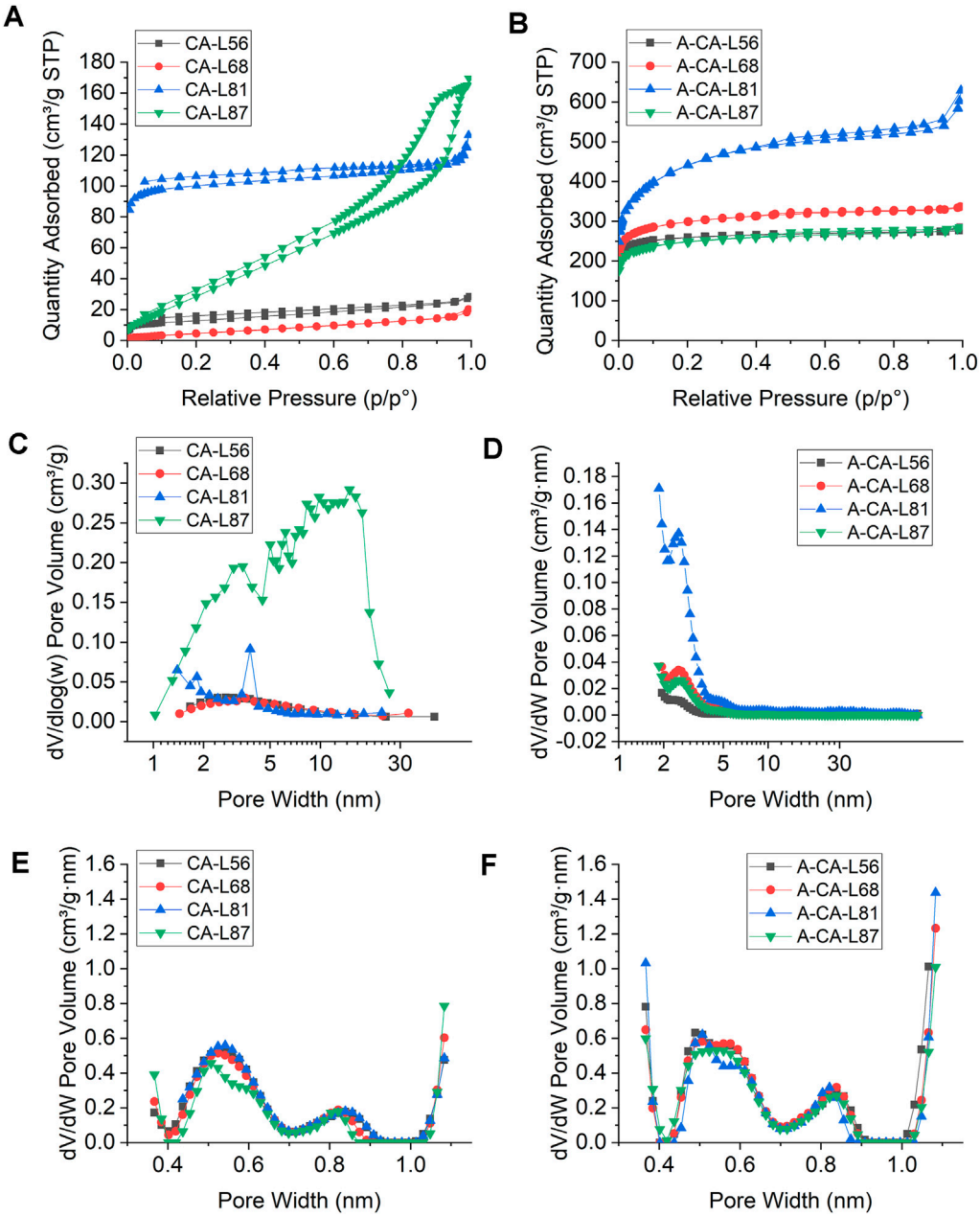

FIGURE 5 | N_2 adsorption-desorption isotherms of **(A)** lignin carbon aerogels (CA) and **(B)** activated carbon aerogels (A-CA) with different lignin contents. Pore size distribution curves of **(C)** CAs using BJH method and **(D)** A-CAs using DFT models determined from N_2 isotherms, size distribution of micropores smaller than 1 nm for **(E)** CAs, **(F)** A-CAs determined using CO_2 adsorption tests.

microporosity with average pore diameters in the range of 2.7–3.4 nm. Moreover, the micropore volumes for the ultra-micropore region increased for all the samples and ranged from 0.36 to 0.44 cm^3/g after activation (**Figure 5F**).

Electrochemical performance of lignin-based carbon aerogels was evaluated through CV and GCD tests in the symmetric two-electrode system. The properties of supercapacitor electrodes fabricated from CA-L87 sample were compared with electrodes assembled from a commercial carbon aerogel (CCA) and activated carbon (A-40), which had BET surface areas of 845 and 1,071 m^2/g, respectively (**Table2**). Based on the XRD and N_2 adsorption results, CA-L87 carbon aerogel was selected for comparison due its higher bulk density, degree of graphitization, total pore volume, and mesoporosity as compared to other samples. The CV curves of the CA-L87, CCA, and A-40 at the 20 mV/s scan rate are shown in **Figure 6A**. The A-40 had a better quasi-rectangular shape, while CA-L87 exhibited a larger area under

TABLE 2 | Surface areas, pore volumes and average pore sizes of lignin carbon aerogels (CA) and activated carbon aerogels (A-CA) with different lignin contents as determined from N_2 and CO_2 gas adsorption isotherms.

	S_{BET}[a] (m^2/g)	S_{micro}[b] (m^2/g)	S_{ext}[c] (m^2/g)	V_{total}[d] (cm^3/g)	V_{micro}[e] (cm^3/g)	d_{pore}[f] (nm)	$V_{micro\text{-}CO_2}$[g] (cm^3/g)
CA-L87	154	106	48	0.26	0.035	4.8	0.29
CA-L81	397	373	25	0.21	0.147	2.7	0.28
CA-L68	21	6	15	0.03	0.004	5.2	0.28
CA-L56	46	29	17	0.04	0.016	4.7	0.27
A-CA-L87	949	920	29	0.44	0.39	2.9	0.36
A-CA-L81	1,609	1,471	138	0.98	0.68	3.4	0.44
A-CA-L68	1,140	1,106	33	0.52	0.47	2.7	0.42
A-CA-L56	1,006	990	16	0.44	0.40	3.1	0.41
A40[h]	1,071	1,048	24	0.51	0.46	2.5	0.29
CCA[i]	845	409	436	3.59	0.16	24	0.27

[a]*Surface area calculated by BET method.*
[b]*Surface area of micropores calculated by t-plot method.*
[c]*External surface area calculated by t-plot method.*
[d]*Total pore volume determined at p/po=0.99 relative pressure.*
[e]*Micropore volume calculated by t-plot method.*
[f]*Average pore diameter calculated from BJH desorption branch.*
[g]*Volume of ultramicropores (<1 nm) calculated by Dubinin method from CO2 adsorption isotherm.*
[h]*Commercial activated carbon.*
[i]*Resorcinol-formaldehyde based commercial carbon aerogel with a bulk density of 0.19 g/cc.*

the CV curve indicating higher specific capacitance (C_s), which were 84.0, 66.6, and 58.7 F/g for CA-L87, CCA, and A-40, respectively. **Figure 6B** shows the CV curves of the CA-L87 sample at different scan rates. The test demonstrated that the shape of the CV curves gradually shifted and tilted with the increase of the scan rate, while the CA-L87 could maintain the quasi-rectangular shape and electrochemical stability even at a higher scan rate of up to 200 mV/s. The C_s of the CA-L87 at 5, 10, 20, 50, 100, and 200 mV/s scan rates were 232.3, 152.7, 88.7, 58.7, 45.5 and 33.4 F/g, respectively. The shape of the charge-discharge curves showed a blunt and slanted quasi-rectangular shape, and the slope of the curves became more pronounced as the scan rate increased. This phenomenon is because of the equivalent series resistance of the electrodes which contain nonconductive binder and other resistive elements within the supercapacitor cells (Mathis et al., 2019). At higher scan rates, the electrolyte ions have a shorter ion migration time to penetrate the pores of the samples, and they are mainly accumulated only on the outer layer surface of electrode (Norouzi et al., 2021). Therefore, the specific capacitance of the CA-L87 decreased with the increase of scan rate. Although the C_s of CA-L87 could reach above 200 F/g at 5 mV/s, it had a 14.4% capacitive retention rate at a 200 mV/s scan rate. In contrast, the CCA and A-40 had lower C_s of 73.9 and 62.5 F/g at 5 mV/s, while they had higher capacitive retention rates of 79.6 and 78.9% at 200 mV/s scan rate, indicating better fast charge-discharge capability.

The GCD curves of CA-L87, CCA, and A-40 at 0.5 A/g current density showed a desired electric double-layer capacitor (EDLC) behavior of linear triangular shapes (**Figure 6C**). The GCD curve of CA-L87 at the different current densities demonstrated that the CA-L87 sample could maintain the symmetric linear triangular shape at 1 A/g current density with a faster charge-discharge rate (**Figure 6D**). The C_s for the CA-L87 sample obtained from the slope of the discharge curves were 263.3, 165.3, and 122.3 F/g at the current density of 0.1, 0.5, and 1 A/g, respectively. The C_s of CA-L87 had a 46.4% capacitive retention when the current density increased from 0.1 to 1 A/g.

Impedance (EIS) tests were also conducted to understand the electrochemical kinetics of the supercapacitor cells. **Figure 6E** shows the Nyquist plots of CA-L87, CCA, and A-40, all of which exhibited typical supercapacitor behavior with a semi-circle at the high-frequency range and a vertical line at the low-frequency range (Liu et al., 2015; Song et al., 2015). The x-intercept of the Nyquist curve represents the equivalent series resistance (R_{es}) of the supercapacitor cell, and the diameter of the semi-circle means the charge-transfer resistance (R_{ct}) from electrolytes moving through the electrodes (Yoo et al., 2014). CA-L87 had the lowest R_{es} (~0.2 Ω) compared to A-40, and CCA samples which also showed low R_{es} values of < 1 Ω. The CA-L87 and A-40 had smaller R_{ct} than CCA, demonstrated higher ion migration rates at the interface between electrolyte and electrode (Wang H. et al., 2016). All the samples had vertical tails at the low-frequency range, which showed good ion accessibility for the electrolyte to penetrate the internal pores. Overall, these observations suggested a lower resistivity of CA-L87 sample, which can be correlated with the N_2 and CO_2 gas adsorption and XRD results showing the existence of both meso- and micropores and higher degree of graphitization. A long cycling life with good stability is critical for the supercapacitor electrode materials (Cao et al., 2021). The capacitive retention test of the CA-L87 sample after 5,000 charge-discharge cycles demonstrated that CA-L87 could still maintain ~90% of its capacitance (**Figure 6F**). The GCD curves had similar behavior after 5,000 cycles, indicating outstanding cycle stability of the CA-L87 and comparable capacitive retention rates with other porous carbon-materials (Chen et al., 2017; Geng et al., 2020; Zhang et al., 2022).

After activation with KOH, the electrochemical performance of the carbon aerogels improved significantly. **Figure 7A** shows

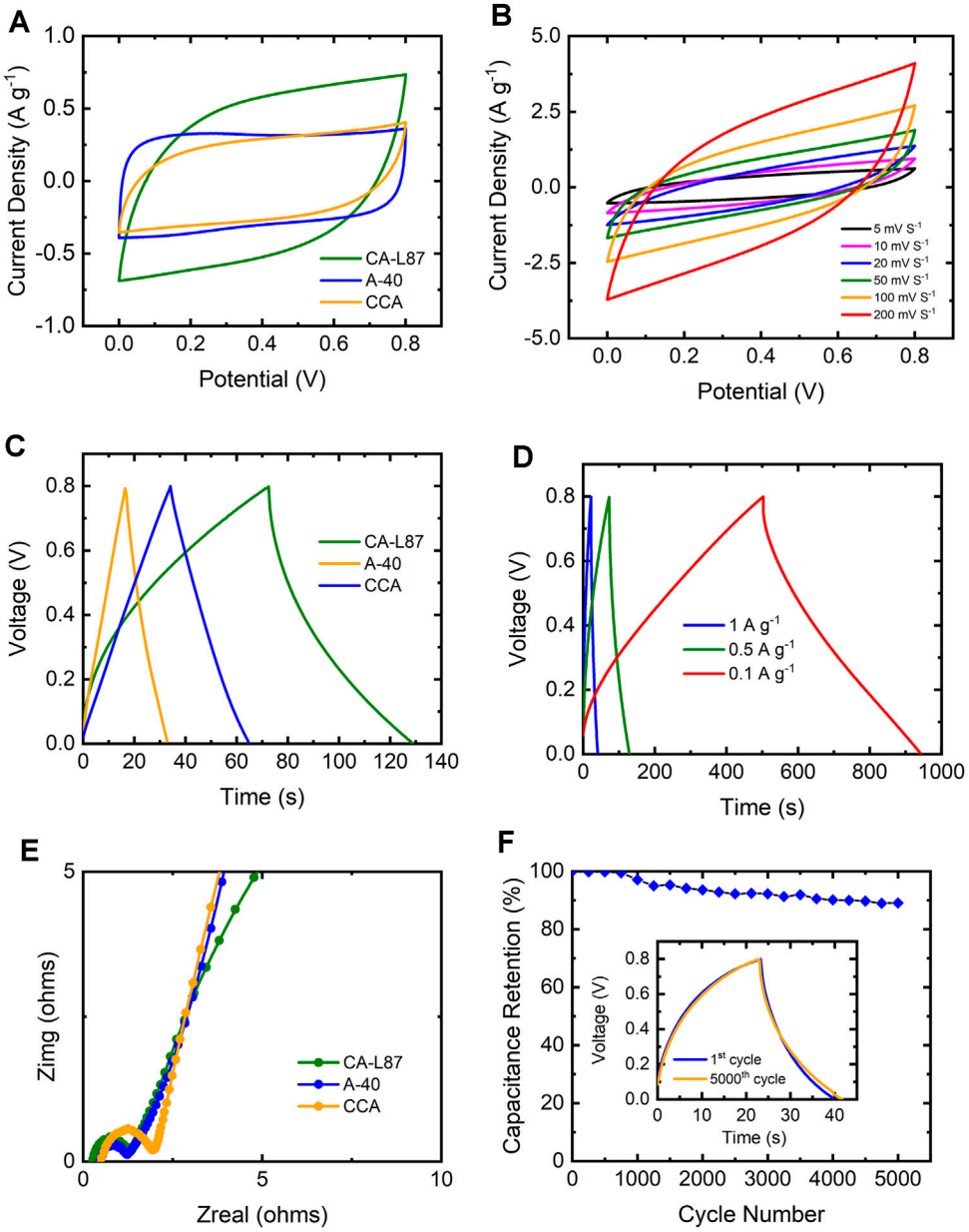

FIGURE 6 | Electrochemical properties of lignin carbon aerogel CA-L87 in comparison to a commercial activated carbon (A40) and a RF-based carbon aerogel (CCA); **(A)** CV curves at the 20 mV s^{-1} scan rate, **(B)** CV curves of CA-L87 with different scan rates, **(C)** GCD curves of the samples at 0.5 Ag^{-1} current density, **(D)** GCD curves of the CA-L87 at different current densities, **(E)** Nyquist plots, **(F)** capacity retention performance of CA-L87 electrode after 5,000 cycles (inset: GCD curve at the 5000th cycle).

that all A-CA samples had symmetric and quasi-rectangular CV curves at a 20 mV/s scan rate, indicating a superior EDLC behavior compared to non-activated CA samples. The C_s of A-CA-L56, A-CA-L68, A-CA-L81 and A-CA-L87 samples obtained from the CV curves at 20 mV/s scan rate were 94.9, 78.2, 108.9, and 130.0 F/g, respectively. For comparison, the C_s of CA-L87 sample improved about 46% after activation at the same CV scan rate (20 mV/s).

The specific capacitance of carbonous materials and the ion transfer and charge storage ability of EDLCs are related not only to the surface area but also to the porous size distribution. In particular, having hierarchical porous structures with a combination of ultra-, micro-, meso-, and macropores is critical to the superior electrochemical performance of carbonous materials (Lin et al., 2019; Thomas et al., 2021). As evidenced by N_2 and CO_2 gas adsorption results, both surface area and total pore volume, especially for the ultramicropores and micropores, of carbon aerogels increased significantly after activation process. As a result, it is suggested that A-CA samples could maintain higher specific capacitance values even

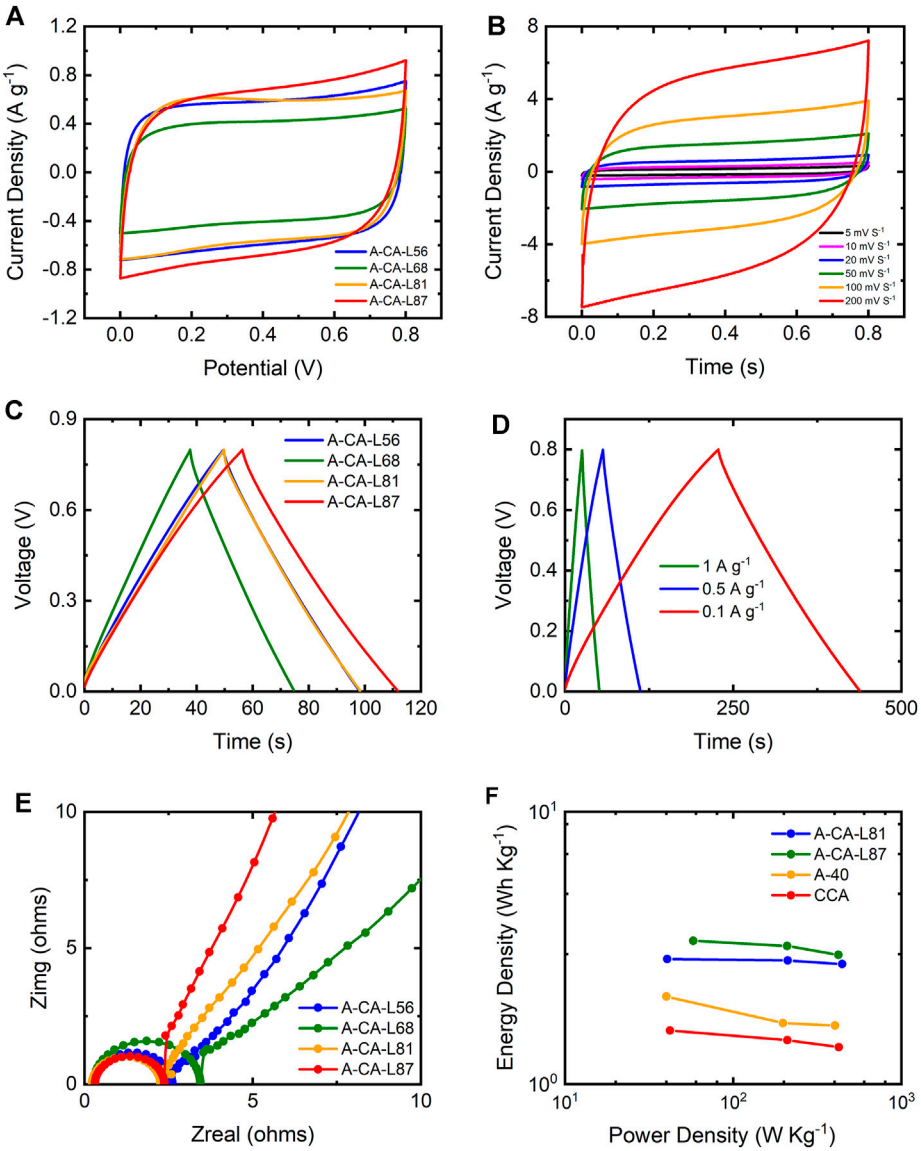

FIGURE 7 | Electrochemical properties of activated lignin carbon aerogels: **(A)** CV curves of the A-CAs with different lignin contents at the 20 mVs^{-1} scan rate and **(B)** CV curves of A-CA-L87 sample with different scan rates; **(C)** GCD curves of the A-CA samples at 0.5 Ag^{-1} current density and **(D)** GCD cures of the A-CA-L87 sample at different current densities; **(E)** Nyquist plots of A-CAs; **(F)** Ragone plots of A-CA-L87, A-CA-L81 in comparison to a commercial activated carbon (A40) and a RF-based carbon aerogel (CCA).

at higher charge-discharge and scan rates compared to non-activated samples.

Figure 7B shows the CV curves of A-CA-L87 at different scan rates. The CV curves could maintain the symmetric quasi-rectangular shape at higher scan rates, and the C_s values calculated for 5, 10, 20, 50, 100, and 200 mV/s were 147.5, 138.6, 130.0, 110.4, 89.4, and 64.7 F/g, respectively. A-CA-L87 sample had a capacity retention rate of 43.9% as the scan rate increased from 5 mV/s to 200 mV/s, which was about three-fold improved performance compared the non-activated CA-L87 sample. As presented in **Figure 7C**, the GCD curves at 0.5 A/g current density indicated a characteristic EDLC linear triangular shape for all A-CA samples. The C_s values calculated with 0.5 A/g discharging current density were 126.4, 96.5, 128.4, and 144.7 F/g for A-CA-L56, A-CA-L68, A-CA-L81 and A-CA-L87 samples, respectively. **Figure 7D** shows the GCD curves of A-CA-L87 at different current densities, at which the C_s values were 151.3 F/g at 0.1 A/g, 144.7 F/g at 0.5 A/g, and 134.2 F/g at 1 A/g. The Cs of A-CA-L87 had a ~88.7% capacitive retention when the current density increased from 0.1 to 1 A/g, which showed a two-fold increase in the performance compared to the non-activated CA-L87 carbon aerogel.

Nyquist plots with a semi-circle at the high-frequency range and a vertical line at the low-frequency range revealed that all

A-CA samples had promising EDLC characteristics (**Figure 7E**). The R_{es} of the A-CA samples were in the range of 0.2–0.4 Ω, and the R_{ct} of the testing samples were in the range of 1.5–2.5 Ω. Interestingly, A-CA-L87 and A-CA-L81 samples, which are activated carbon aerogels with higher lignin contents, had smaller semi-circles with a more vertical tail line, indicating lower R_{es} and R_{ct} with better ion accessibility. The Ragone plot of A-CA-L87 and A-CA-L81 activated carbon aerogels in comparison to a commercial activated carbon (A40) and a RF-based carbon aerogel (CCA) is shown in **Figure 7F**. A-CA-L87 and A-CA-L81 had an outstanding energy and power densities, 3.2 Wh/kg at 209.1 W/kg and 2.9 Wh/kg at 210.8 W/kg, respectively, which were better than CCA (1.5 Wh/kg at 209.6 W/kg) and A-40 (1.7 Wh/kg at 197.3 W/kg) at a similar power density range. These results demonstrated that ACA-L87 and ACA-L81 activated carbon aerogels are promising candidates as supercapacitor electrodes.

CONCLUSIONS

In this study, biomass-derived low-cost carbon aerogels suitable for energy storage applications were fabricated using an industrial softwood kraft lignin isolated from renewable forest resources. Lignin-epoxy based gels with high lignin contents were synthesized without using toxic and expensive organic precursors such as resorcinol, phenol, and formaldehyde and converted into carbon aerogel products using sol-gel processing, supercritical drying and pyrolysis. Results showed that depending on the lignin-to-crosslinker ratio, the chemical, physical, and structural properties of carbon aerogels and the electrochemical energy storage performance of carbon electrodes fabricated from these carbon aerogels can be fine-tuned. The bulk density (up to 0.83 g/cm^3) and carbonization yield (up to 47%) of carbon aerogels increased as the lignin content increased from 56 to 87 wt%. FTIR analysis showed that increasing the amount of crosslinker favored formation of epoxidized lignin rather than crosslinked network structure, which altered the surface morphology and porous structure of carbon aerogels. XRD results demonstrated that the degree of graphitization improved with increasing the lignin content, suggesting better electrical conductivity and lower charge-transfer resistance and superior EDLC performance for the CA-L87 carbon aerogel. SEM analysis and N_2 adsorption-desorption isotherms together with CO_2 adsorption results revealed that lignin carbon aerogels had hierarchical porosity including of micro-, meso- and macropores in addition to ultramicropores less than 1 nm. Moreover, chemical activation with KOH significantly improved the pore textural properties of carbon aerogels introducing additional microporosity, surface area and pore volume. As a result, BET surface area, total pore volume and micropore volume with values reached up to 1,609 m^2/g and 0.98 cm^3/g with 0.68 cm^3/g, respectively. The supercapacitor electrodes fabricated from CA-L87 carbon aerogel showed a specific capacitance of 122 F/g at 1 A/g and ~90% capacitance retention after 5,000 charge-discharge cycles, superior electrochemical performance and cyclic stability as compared to a commercial activated carbon and RF-based carbon aerogel tested using the same two-electrode system. In addition, surface activation further improved the EDLC performance, specific capacitance, capacitive rate retention, which is attributed to the changes to internal pore structure of carbon aerogels. The assembled symmetric supercapacitor cells from the activated carbon aerogel with 87% lignin content had an outstanding energy density of 3.2 Wh/kg at 209.1 W/kg power density. These results suggested that lignin-epoxy based activated carbon aerogels are promising low-cost renewable materials for energy applications, not only for supercapacitors but also for carbon electrodes used in other hybrid battery systems such as Li-ion capacitors (Niu et al., 2018).

DATA AVAILABILITY STATEMENT

The raw data supporting the conclusions of this article will be made available by the authors, without undue reservation.

AUTHOR CONTRIBUTIONS

MK: Conceptualization, Methodology, Data collection and validation, Data analysis, Visualization, Investigation, Writing original draft, Review editing. LL: Data collection and validation, Formal analysis, Investigation, Writing original draft, Review editing. FK: Conceptualization, Resources, Supervision, Funding acquisition, Review editing. SR: Conceptualization, Methodology, Resources, Supervision, Funding acquisition, Review editing the original draft. All authors have read and agreed to the published version of the manuscript.

FUNDING

The work was supported by the Natural Sciences and Engineering Research Council of Canada (NSERC) Collaborative Research and Development (CRD) project #CRDPJ 529966–18 in collaboration with Domtar Inc. Also, support from the Advanced Renewable Materials Innovation Fund, sponsored by the Paul and Edwina Heller Memorial Fund and by the Canada Research Chairs Program, Tier 2, in Advanced Renewable Materials #950–232330.

ACKNOWLEDGMENTS

The authors acknowledge key insights and discussions by Bruno Marcoccia and Shabnam Sanaei during the length of the project.

REFERENCES

Ambroz, F., Macdonald, T. J., Martis, V., and Parkin, I. P. (2018). Evaluation of the BET Theory for the Characterization of Meso and Microporous MOFs. *Small Methods* 2, 1800173. doi:10.1002/smtd.201800173

Antonietti, M., Fechler, N., and Fellinger, T.-P. (2014). Carbon Aerogels and Monoliths: Control of Porosity and Nanoarchitecture via Sol-Gel Routes. *Chem. Mat.* 26, 196–210. doi:10.1021/cm402239e

Baker, D. A., and Rials, T. G. (2013). Recent Advances in Low-Cost Carbon Fiber Manufacture from Lignin. *J. Appl. Polym. Sci.* 130, 713–728. doi:10.1002/app.39273

Baldino, L., Zuppolini, S., Cardea, S., Diodato, L., Borriello, A., Reverchon, E., et al. (2020). Production of Biodegradable Superabsorbent Aerogels Using a Supercritical CO2 Assisted Drying. *J. Supercrit. Fluids* 156, 104681. doi:10.1016/j.supflu.2019.104681

Biener, J., Stadermann, M., Suss, M., Worsley, M. a., Biener, M. M., Rose, K. a., et al. (2011). Advanced Carbon Aerogels for Energy Applications. *Energy Environ. Sci.* 4, 656. doi:10.1039/c0ee00627k

Cao, Y., Yang, W., Wang, M., Wu, N., Zhang, L., Guan, Q., et al. (2021). Metal-organic Frameworks as Highly Efficient Electrodes for Long Cycling Stability Supercapacitors. *Int. J. Hydrogen Energy* 46, 18179–18206. doi:10.1016/j.ijhydene.2021.03.003

Castro-Gutiérrez, J., Celzard, A., and Fierro, V. (2020). Energy Storage in Supercapacitors: Focus on Tannin-Derived Carbon Electrodes. *Front. Mater.* 7, 217. Available at: https://www.frontiersin.org/article/10.3389/fmats.2020.00217 (Accessed March 9, 2022). doi:10.3389/fmats.2020.00217

Chen, F., Min, X., Lijuan, W., and Jian, L. (2011). Preparation and Characterization of Organic Aerogels by the Lignin-Resorcinol-Formaldehyde Copolymer. *BioResources* 6, 1262–1272.doi:10.15376/biores.6.2.1262-1272

Chen, X., Paul, R., and Dai, L. (2017). Carbon-based Supercapacitors for Efficient Energy Storage. *Natl. Sci. Rev.* 4, 453–489. doi:10.1093/nsr/nwx009

Collins, M. N., Nechifor, M., Tanasă, F., Zănoagă, M., McLoughlin, A., Stróżyk, M. A., et al. (2019). Valorization of Lignin in Polymer and Composite Systems for Advanced Engineering Applications - A Review. *Int. J. Biol. Macromol.* 131, 828–849. doi:10.1016/j.ijbiomac.2019.03.069

Culebras, M., Collins, G. A., Beaucamp, A., Geaney, H., and Collins, M. N. (2022). Lignin/Si Hybrid Carbon Nanofibers towards Highly Efficient Sustainable Li-Ion Anode Materials. *Eng. Sci.* 17, 195–203. doi:10.30919/es8d608

Deka, B. K., Hazarika, A., Kim, J., Park, Y.-B., and Park, H. W. (2017). Recent Development and Challenges of Multifunctional Structural Supercapacitors for Automotive Industries. *Int. J. Energy Res.* 41, 1397–1411. doi:10.1002/er.3707

Gao, Z., Zhang, Y., Song, N., and Li, X. (2017). Biomass-derived Renewable Carbon Materials for Electrochemical Energy Storage. *Mater. Res. Lett.* 5, 69–88. doi:10.1080/21663831.2016.1250834

Geng, S., Wei, J., Jonasson, S., Hedlund, J., and Oksman, K. (2020). Multifunctional Carbon Aerogels with Hierarchical Anisotropic Structure Derived from Lignin and Cellulose Nanofibers for CO2 Capture and Energy Storage. *ACS Appl. Mat. Interfaces* 12, 7432–7441. doi:10.1021/acsami.9b19955

Glasser, W. G. (2019). About Making Lignin Great Again-Some Lessons from the Past. *Front. Chem.* 7, 565. doi:10.3389/fchem.2019.00565

González, A., Goikolea, E., Barrena, J. A., and Mysyk, R. (2016). Review on Supercapacitors: Technologies and Materials. *Renew. Sustain. Energy Rev.* 58, 1189–1206. doi:10.1016/j.rser.2015.12.249

Grishechko, L. I., Amaral-Labat, G., Szczurek, A., Fierro, V., Kuznetsov, B. N., and Celzard, A. (2013b). Lignin-phenol-formaldehyde Aerogels and Cryogels. *Microporous Mesoporous Mater.* 168, 19–29. doi:10.1016/j.micromeso.2012.09.024

Grishechko, L. I., Amaral-Labat, G., Szczurek, a., Fierro, V., Kuznetsov, B. N., Pizzi, a., et al. (2013a). New Tannin-Lignin Aerogels. *Industrial Crops Prod.* 41, 347–355. doi:10.1016/j.indcrop.2012.04.052

Jin, H., Li, J., Yuan, Y., Wang, J., Lu, J., and Wang, S. (2018). Recent Progress in Biomass-Derived Electrode Materials for High Volumetric Performance Supercapacitors. *Adv. Energy Mat.* 8, 1801007. doi:10.1002/aenm.201801007

Ko, K.-J., Jin, S., Lee, H., Kim, K.-M., Mofarahi, M., and Lee, C.-H. (2021). Role of Ultra-micropores in CO2 Adsorption on Highly Durable Resin-Based Activated Carbon Beads by Potassium Hydroxide Activation. *Ind. Eng. Chem. Res.* 60, 14547–14563. doi:10.1021/acs.iecr.1c02430

Li, F., Xie, L., Sun, G., Kong, Q., Su, F., Cao, Y., et al. (2019a). Resorcinol-formaldehyde Based Carbon Aerogel: Preparation, Structure and Applications in Energy Storage Devices. *Microporous Mesoporous Mater.* 279, 293–315. doi:10.1016/j.micromeso.2018.12.007

Li, J., Yan, Q., Zhang, X., Zhang, J., and Cai, Z. (2019b). Efficient Conversion of Lignin Waste to High Value Bio-Graphene Oxide Nanomaterials. *Polymers* 11, 623. doi:10.3390/polym11040623

Lin, J., Xue, F., and Zhao, G. (2019). Soda Lignin-Based Activated Carbon and its Adsorption Properties. *BioResources* 14, 376–386. doi:10.15376/biores.14.1.376-386

Liu, L.-Y., Bessler, K., Chen, S., Cho, M., Hua, Q., and Renneckar, S. (2020). Data on Making Uniform Lignin Building Blocks via *In-Situ* Real-Time Monitoring of Hydroxyethyl Modification. *Data Brief* 33, 106512. doi:10.1016/j.dib.2020.106512

Liu, R., Pan, L., Liu, X., and Wu, D. (2015). An Evaporation-Induced Tri-constituent Assembly Approach to Fabricate an Ordered Mesoporous Carbon/graphene Aerogel for High-Performance Supercapacitors. *RSC Adv.* 5, 16765–16768. doi:10.1039/C4RA13720E

Ma, Y., Chen, D., Fang, Z., Zheng, Y., Li, W., Xu, S., et al. (2021). High Energy Density and Extremely Stable Supercapacitors Based on Carbon Aerogels with 100% Capacitance Retention up to 65,000 Cycles. *Proc. Natl. Acad. Sci.* 118, e2105610118. doi:10.1073/pnas.2105610118

Mathis, T. S., Kurra, N., Wang, X., Pinto, D., Simon, P., and Gogotsi, Y. (2019). Energy Storage Data Reporting in Perspective-Guidelines for Interpreting the Performance of Electrochemical Energy Storage Systems. *Adv. Energy Mat.* 9, 1902007. doi:10.1002/aenm.201902007

Meynen, V., Cool, P., and Vansant, E. F. (2009). Verified Syntheses of Mesoporous Materials. *Microporous Mesoporous Mater.* 125, 170–223. doi:10.1016/j.micromeso.2009.03.046

Mundt, K. A., Gentry, P. R., Dell, L. D., Rodricks, J. V., and Boffetta, P. (2018). Six Years after the NRC Review of EPA's Draft IRIS Toxicological Review of Formaldehyde : Regulatory Implications of New Science in Evaluating Formaldehyde Leukemogenicity. *Regul. Toxicol. Pharmacol.* 92, 472–490. doi:10.1016/j.yrtph.2017.11.006

Niu, J., Shao, R., Liu, M., Liang, J., Zhang, Z., Dou, M., et al. (2018). Porous Carbon Electrodes with Battery-Capacitive Storage Features for High Performance Li-Ion Capacitors. *Energy Storage Mater.* 12, 145–152. doi:10.1016/j.ensm.2017.12.012

Norouzi, O., Pourhosseini, S. E. M., Naderi, H. R., Di Maria, F., and Dutta, A. (2021). Integrated Hybrid Architecture of Metal and Biochar for High Performance Asymmetric Supercapacitors. *Sci. Rep.* 11, 5387. doi:10.1038/s41598-021-84979-z

Nypelö, T. E., Carrillo, C. A., and Rojas, O. J. (2015). Lignin Supracolloids Synthesized from (W/O) Microemulsions: Use in the Interfacial Stabilization of Pickering Systems and Organic Carriers for Silver Metal. *Soft Matter* 11, 2046–2054. doi:10.1039/c4sm02851a

Palchoudhury, S., Ramasamy, K., Gupta, R. K., and Gupta, A. (2019). Flexible Supercapacitors: A Materials Perspective. *Front. Mater.* 5, 83. Available at: https://www.frontiersin.org/article/10.3389/fmats.2018.00083 (Accessed March 9, 2022). doi:10.3389/fmats.2018.0008310.3389/fmats.2018.00083

Passauer, L., Chemistry, W., and Dresden, T. U. (2012). Highly Swellable Lignin Hydrogels. *ACS Symp. Ser.*, 1107, 211–228. doi:10.1021/bk-2012-1107.ch011

Ragauskas, A. J., Beckham, G. T., Biddy, M. J., Chandra, R., Chen, F., Davis, M. F., et al. (2014). Lignin Valorization: Improving Lignin Processing in the Biorefinery. *Science* 344, 1246843. doi:10.1126/science.1246843

Raza, W., Ali, F., Raza, N., Luo, Y., Kim, K.-H., Yang, J., et al. (2018). Recent Advancements in Supercapacitor Technology. *Nano Energy* 52, 441–473. doi:10.1016/j.nanoen.2018.08.013

Romanos, J., Beckner, M., Rash, T., Firlej, L., Kuchta, B., Yu, P., et al. (2011). Nanospace Engineering of KOH Activated Carbon. *Nanotechnology* 23, 015401. doi:10.1088/0957-4484/23/1/015401

Rovira, J., Roig, N., Nadal, M., Schuhmacher, M., and Domingo, J. L. (2016). Human Health Risks of Formaldehyde Indoor Levels: An Issue of Concern. *J. Environ. Sci. Health, Part A* 51, 357–363. doi:10.1080/10934529.2015.1109411

Saidane, D., Barbe, J.-C., Birot, M., and Deleuze, H. (2009). Preparation of Functionalized Kraft Lignin Beads. *J. Appl. Polym. Sci.* 116, a–n. doi:10.1002/app.31659

Sam, D. K., Sam, E. K., Durairaj, A., Lv, X., Zhou, Z., and Liu, J. (2020). Synthesis of Biomass-Based Carbon Aerogels in Energy and Sustainability. *Carbohydr. Res.* 491, 107986. doi:10.1016/j.carres.2020.107986

Song, W.-L., Song, K., and Fan, L.-Z. (2015). A Versatile Strategy toward Binary Three-Dimensional Architectures Based on Engineering Graphene Aerogels with Porous Carbon Fabrics for Supercapacitors. *ACS Appl. Mat. Interfaces* 7, 4257–4264. doi:10.1021/am508624x

Szczurek, A., Amaral-Labat, G., Fierro, V., Pizzi, A., Masson, E., and Celzard, A. (2011). The Use of Tannin to Prepare Carbon Gels. Part I: Carbon Aerogels. *Carbon* 49, 2773–2784. doi:10.1016/j.carbon.2011.03.007

Tamborini, L., Militello, P., Barbero, C., Acevedo, D., and Acevedo, D. (2017). Production of Porous Carbons from Resorcinol-Formaldehyde Gels: Applications. *Handb. Compos. Renew. Mater.* 1–8, 175–196. doi:10.1002/9781119441632.ch26

Tao, Y., Xie, X., Lv, W., Tang, D.-M., Kong, D., Huang, Z., et al. (2013). Towards Ultrahigh Volumetric Capacitance: Graphene Derived Highly Dense but Porous Carbons for Supercapacitors. *Sci. Rep.* 3, 2975. doi:10.1038/srep02975

Thomas, B., Geng, S., Sain, M., and Oksman, K. (2021). Hetero-porous, High-Surface Area Green Carbon Aerogels for the Next-Generation Energy Storage Applications. *Nanomaterials* 11, 653–719. doi:10.3390/nano11030653

Thommes, M., and Cychosz, K. A. (2014). Physical Adsorption Characterization of Nanoporous Materials: Progress and Challenges. *Adsorption* 20, 233–250. doi:10.1007/s10450-014-9606-z

Wang, H., Yu, S., and Xu, B. (2016a). Hierarchical Porous Carbon Materials Prepared Using Nano-ZnO as a Template and Activation Agent for Ultrahigh Power Supercapacitors. *Chem. Commun.* 52, 11512–11515. doi:10.1039/C6CC05911B

Wang, J., and Kaskel, S. (2012). KOH Activation of Carbon-Based Materials for Energy Storage. *J. Mat. Chem.* 22, 23710–23725. doi:10.1039/C2JM34066F

Wang, Q., Yan, J., and Fan, Z. (2016b). Carbon Materials for High Volumetric Performance Supercapacitors: Design, Progress, Challenges and Opportunities. *Energy Environ. Sci.* 9, 729–762. doi:10.1039/C5EE03109E

Xu, J., Zhou, X., Chen, M., Shi, S., and Cao, Y. (2018). Preparing Hierarchical Porous Carbon Aerogels Based on Enzymatic Hydrolysis Lignin through Ambient Drying for Supercapacitor Electrodes. *Microporous Mesoporous Mater.* 265, 258–265. doi:10.1016/j.micromeso.2018.02.024

Xu, X., Zhou, J., Nagaraju, D. H., Jiang, L., Marinov, V. R., Lubineau, G., et al. (2015). Flexible, Highly Graphitized Carbon Aerogels Based on Bacterial Cellulose/lignin: Catalyst-free Synthesis and its Application in Energy Storage Devices. *Adv. Funct. Mat.* 25, 3193–3202. doi:10.1002/adfm.201500538

Yang, B. S., Kang, K.-Y., and Jeong, M.-J. (2017). Preparation of Lignin-Based Carbon Aerogels as Biomaterials for Nano-Supercapacitor. *J. Korean Phys. Soc.* 71, 478–482. doi:10.3938/jkps.71.478

Yoo, H. D., Jang, J. H., Ryu, J. H., Park, Y., and Oh, S. M. (2014). Impedance Analysis of Porous Carbon Electrodes to Predict Rate Capability of Electric Double-Layer Capacitors. *J. Power Sources* 267, 411–420. doi:10.1016/j.jpowsour.2014.05.058

Zhang, D., Tan, C., Zhang, W., Pan, W., Wang, Q., and Li, L. (2022). Expanded Graphite-Based Materials for Supercapacitors: A Review. *Molecules* 27, 716. doi:10.3390/molecules27030716

Zhang, X., Yan, Q., Leng, W., Li, J., Zhang, J., Cai, Z., et al. (2017). Carbon Nanostructure of Kraft Lignin Thermally Treated at 500 to 1000 °C. *Materials* 10, 975. doi:10.3390/ma10080975

Zhu, J., Yan, C., Zhang, X., Yang, C., Jiang, M., and Zhang, X. (2020). A Sustainable Platform of Lignin: From Bioresources to Materials and Their Applications in Rechargeable Batteries and Supercapacitors. *Prog. Energy Combust. Sci.* 76, 100788. doi:10.1016/j.pecs.2019.100788

Conflict of Interest: The authors declare that the research was conducted in the absence of any commercial or financial relationships that could be construed as a potential conflict of interest.

Publisher's Note: All claims expressed in this article are solely those of the authors and do not necessarily represent those of their affiliated organizations, or those of the publisher, the editors and the reviewers. Any product that may be evaluated in this article, or claim that may be made by its manufacturer, is not guaranteed or endorsed by the publisher.